InP quantum dots embedded in GaP: Optical properties and carrier dynamics

F. Hatami* and W. T. Masselink
Department of Physics, Humboldt-Universität zu Berlin, Invalidenstrasse 110, Berlin 10115, Germany

L. Schrottke
Paul-Drude-Institut für Festkörperelektronik, Hausvogteiplatz 5-7, Berlin 10117, Germany

J. W. Tomm and V. Talalaev
Max-Born-Institut für Nichtlineare Optik und Kurzzeitspektroskopie, Max-Born-Strasse 2A, Berlin 12489, Germany

C. Kristukat and A. R. Goñi
Institut für Festkörperphysik, Technische Universität Berlin, Hardenbergstrasse 36, Berlin 10623, Germany
(Received 30 October 2002; published 5 February 2003)

The optical emission and dynamics of carriers in Stranski-Krastanow self-organized InP quantum dots embedded in a GaP matrix are studied. InP deposited on GaP (001) using gas-source molecular-beam epitaxy forms quantum dots for InP coverage greater than 1.8 monolayers. Strong photoluminescence from the quantum dots is observed up to room temperature at about 2 eV; photoluminescence from the two-dimensional InP wetting layer is measured at about 2.2 eV. Modeling based on the ''model-solid theory'' indicates that the band alignment for the InP quantum dots is direct and type I. Furthermore, low-temperature time-resolved photoluminescence measurements indicate that the carrier lifetime in the quantum dots is about 2 ns, typical for type-I quantum dots. Pressure-dependent photoluminescence measurements provide further evidence for a type-I band alignment for InP/GaP quantum dots at normal pressure with the GaP *X* states lying about 30 meV higher than the Γ states in the InP quantum dots, but indicate that they become type II under hydrostatic pressures of about 1.2 GPa.

DOI: 10.1103/PhysRevB.67.085306 PACS number(s): 73.20.Fz, 73.61.Ey, 73.63.Nm, 81.15.Hi

I. INTRODUCTION

Fabrication of self-organized quantum dots (QD's) using the coherent-island Stranski-Krastanow growth mode has been realized in a number of material systems, the most extensively investigated of which is that of InAs QD's on and in GaAs. The material system of InP QD's on GaP has been much less extensively investigated than InAs/GaAs, but is interesting both for a fundamental understanding of the physics of QD formation and for its potential applications to visible light emitters. Quantum-dot formation in InP/GaP system due to the self-organized growth mechanism is expected under the proper growth conditions, driven by the 7.7% lattice mismatch between strained InP and GaP. Following the analogy to InAs/GaAs, the wider band gaps of the InP and GaP should result in optical emission from the InP dots near 2 eV. The realization of such emission is potentially of great importance because it could allow high efficiency direct recombination in the InP QD's within a GaP matrix and on a GaP substrate, taking advantage of the well-developed GaP-based light-emitting diode (LED) technology. Furthermore, using the transparent GaP rather than GaAs as substrate allows easier extraction of the emitted light for vertical structures such as superluminescent LED's or vertical cavity lasers.

The growth of large (400 nm in base size and 100 nm in height) partially relaxed InP islands on GaP using organometallic vapor-phase epitaxy (MOVPE) after deposition of about 1.2 monolayers (ML) InP is reported in Ref. 1. Likewise, Junno *et al.* reported the formation of relaxed InP QD's on GaP after deposition of about 3-ML InP using chemical beam epitaxy;[2] according to their studies, the height of islands varied between 5 and 20 nm. InAs QD's have also been realized on (001) GaP substrates, apparently forming in the Volmer-Weber mode and luminescing at about 1.7 eV.[3] We have recently described the formation of InP QD's using gas-source molecular-beam epitaxy (GSMBE);[4] in contrast with other reports, however, we are able to achieve intense optical emission from the GSMBE-prepared InP QD's.[5] Junno *et al.* attributed the lack of luminescence in large QD's to the large strain in the system, which could change the conduction-band alignment to separate the electrons and holes in the InP/GaP QD system.[2]

In the present paper, we describe in detail the optical characterization and carrier dynamics in InP quantum dots in GaP grown by GSMBE. Using time-resolved photoluminescence and pressure-dependent photoluminescence, we show that the InP/GaP QD system is type I, so that both electrons and holes are confined in the InP QD's, leading to strong carrier recombination and intense light emission. This result is in contrast with a recent theoretical investigation,[6] but consistent with the model-solid theory of Van de Walle.[7]

II. GROWTH AND ANALYSIS TECHNIQUES

A. Growth

Structures are grown using GSMBE on (001)-GaP substrates in a Riber-32-P molecular beam epitaxy system. After oxide desorption, a 200-nm-GaP buffer layer is grown at 565 °C at a rate of 0.9 μm/h. The growth is then interrupted

while the substrate temperature is reduced. Subsequently, the desired coverage of InP is deposited at 410–490 °C, followed by a growth interruption of 60 s. The InP growth rate has been varied between 0.08 and 0.22 μm/h for different samples. Each sample contains one to nine periods InP/GaP with InP coverage between 1.8 and 5.8 ML and intervening GaP barrier thickness of 5–20 nm, dependent on sample. We measure the InP coverage on the GaP surface in ML taking into consideration the enlargement of the vertical InP lattice constant under compressive in-plane strain (6.730×10^{14} indium atoms/cm^2 in a compressed monolayer). The resulting structures are then capped with GaP. The growth process is monitored using reflection high-energy electron diffraction (RHEED); during GaP growth, the surface shows a (2×4) reconstruction. At the beginning of InP growth, the RHEED pattern appears streaky, indicating two-dimensional (2D) growth, and gradually becomes spotty and less intense after the deposition of about 1.8 ML of InP (3D growth). Samples prepared for atomic force microscopy and scanning electron microscopy studies were grown without cap layer.

B. Structural and optical analysis techniques

The structural properties of the samples have been characterized using double-crystal x-ray diffractometry, scanning electron microscopy (SEM), transmission electron microscopy (TEM), and atomic force microscopy (AFM). X-ray rocking curves were examined for the (004) reflection using Cu $K\alpha_1$ radiation with a resolution of about 10″. SEM studies have been conducted in a S360 Leica Cambridge microscope and AFM investigations have been carried out in a TopoMetrix discover microscope. Additionally, samples have been studied in cross section and plan view by TEM in a Hitachi H-8110 microscope operated at 200 keV.

Photoluminescence is excited using the 325 nm line of a He-Cd laser. The emission is dispersed by a 1 m monochromator and detected by a charge-coupled device camera. The measurements are performed in the temperature range of 5–300 K.

For the time-resolved photoluminescence (PL) for times up to about 2000 ps, excitation laser pulses shorter than 100 fs are generated by a frequency-doubled Spectra Physics Tsunami Ti:Sapphire-laser pumped by an Ar^+ laser. The excitation wavelength is 395 nm and the repetition rate 82 MHz. The PL emission is measured using a 0.25-m-grating monochromator and a Hamamatsu synchroscan streak camera. Nonequilibrium carrier densities up to $\delta n=10^{16}$ cm^{-3} are generated by each pulse. The overall temporal resolution of this configuration is better than 20 ps. For time-resolved measurements up to 20 ns, the configuration was as described in Ref. 8.

The photoluminescence has also been investigated under hydrostatic pressure up to 10 GPa. For these experiments, the samples are chemically thinned to a total thickness of about 30 μm and then cut into pieces of about 100×100 μm^2. The measurements are performed at 4 K using a diamond-anvil cell and the luminescence is excited using the 488 nm line of an Ar^+ laser.

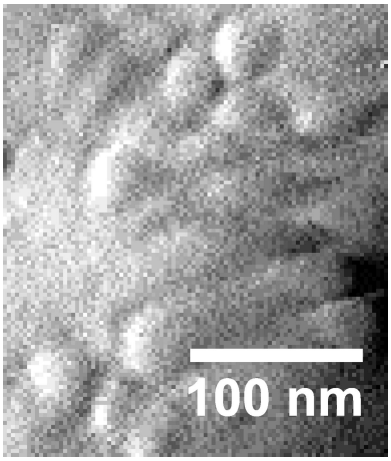

FIG. 1. AFM micrograph of a sample containing 3-ML InP grown under high-PH_3 flux.

III. RESULTS AND DISCUSSION

A. Structural properties

Both the *in situ* RHEED measurements and the AFM studies indicate that dot formation begins after deposition of about 1.8 ML of InP.[5] While the critical deposition for island formation appears to be independent of growth conditions, the size and the area density of the dots are particularly dependent on the PH_3 flux.

InP deposition using a relatively low-PH_3 flux of about 1.1 sccm (standard cubic centimeter per minute), results in InP islands with quite large lateral sizes; AFM measurements show average lateral sizes from 100 to 130 nm as the InP coverage is increased from 2 to 6 ML. The dot density changes in the range of $(2-6)\times10^8$ cm^{-2} and the average height of the dots is about 18–20 nm and nearly independent of InP coverage. These large dots form under low-PH_3 flux even at deposition rates as low as 0.08 ML/s and a substrate temperature of 450 °C. Furthermore, AFM images reveal that the large islands grown at lower-PH_3 flux composed of 2–4 smaller dots that have conglomerated; a detailed statistical analysis shows no indication, however, of a multimodal size distribution. Preference for cluster nucleation may be here either because of reduction of the surface energy (Oswald ripening) or because of already existing dots. Furthermore, the formation of the large InP/GaP QD's compared to other highly lattice-mismatched III–V QD's may be explained by the large elastic constants in bulk InP. The total strain energy in the continuum mechanical model is proportional to the elastic constant and the square of the lattice-mismatch degree.[9] Due to larger elastic constants in bulk InP than in bulk InAs,[10] a higher strain energy in the InP/GaP system is expected, which should lead to earlier strain relaxation and larger dots.

Higher-PH_3 flux during InP deposition leads, however, to smaller islands. This effect was also observed for InP/GaP MOVPE islands[1] and a similar effect is seen in the InAs/GaAs system.[11] Figure 1 shows an AFM image from a sample containing 3-ML InP grown under PH_3 flux of about 1.7 sccm (high flux) at a substrate temperature of 490 °C. The dots in this sample are significantly smaller than those

TABLE I. Area density, base length, and height of InP QD's as function of PH_3 flux based on AFM data. The InP coverage is about 3 ML.

PH_3 Flux (sccm)	Areal density ($dots/cm^2$)	Base length (nm)	Height (nm)
1.1	2×10^8	100	18
1.7	2×10^{10}	25	3

grown under the low-PH_3 flux condition because the higher-PH_3 flux leads to a higher phosphorus surface density and lower in-surface mobility. Both AFM and TEM studies indicate that the average base length of QD's for samples containing 2-ML InP and grown under high-PH_3 flux is about 20 nm; the height of the dots, according to high-resolution TEM, is between 3 and 5 nm. The higher-PH_3 flux results not only in smaller dot size, but, correspondingly, in an increase of QD areal density. The size and density data for two samples with 3-ML-InP coverage, but with different PH_3 fluxes are compiled in Table I.

Besides the structural differences between the InP QD's grown under differing PH_3 fluxes, we obtain photoluminescence only from the smaller QD's grown under higher-PH_3 flux. In our experiments, the lateral cutoff size for obtaining optical emission is about 50 nm, perhaps due to nonradiative recombination centers in the dots. A further reason can be the complicated band alignment of the InP dots with the GaP matrix which depends on the dot geometry and strain, leading to a system which can be indirect in both **k** and real space. The lack of luminescence from the larger dots is also consistent with other results in this material system.[1,2] The issue of direct transitions versus indirect transitions will be discussed in the following section.

B. Electronic structure

Optical properties are determined by the electronic structure, which is strongly dependent on both the structural properties of the InP quantum dots and on strain. The band alignment, including strain effects, is estimated using the model-solid theory by Van de Walle.[7] Using the estimated band alignment, we calculate the localization energies for both electrons and heavy holes as functions of InP thickness. Since the lateral dimensions of the QD's are much larger than their vertical dimensions, we neglect the energetic shift due lateral confinement effects and model the QD's as weak laterally confined quasi-two-dimensional slices. Within a multivalley effective-mass approximation, we find that for the coupled InP/GaP quantum wells (QW's) with InP coverage thinner than about 3 nm (8.5 ML), the Γ-like electrons in InP layer are located at a higher energy than the X states in the GaP layer — for instance, in the case of ultrathin QW (thinner than 1 nm) the Γ-like electrons in the InP layer are about 500 meV higher in energy than GaP X states — leading to localization of electrons in the X valley in the GaP. Hence, the structure is type II. This situation is experimentally realized in the InP QW's.[8] The effect of the biaxial strain in the InP is to split the X states, with the X_{xy} states

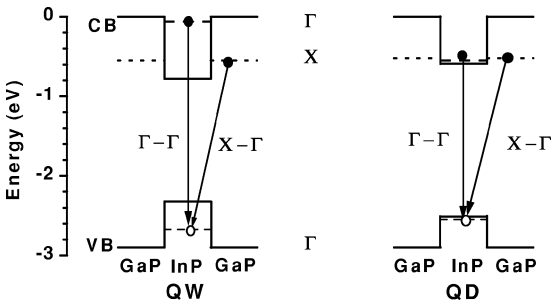

FIG. 2. Valence and conduction-band alignment schema of the pseudomorphic InP/GaP MQW and QD. The arrows indicate the two possibilities of electron-hole recombination.

being pushed to lower energies near the size-quantized Γ-state energy. The InP L states are not expected to play any role because they are not significantly lowered in energy in (001) strained systems. We estimate that for thin wells, the lowest-energy states are the X states of the GaP, but that the X_{xy} states of the InP could also play a role. In the case of the wetting layer, the situation is even more complicated because of possible coupling with the QD states.

The calculations based on the model-solid theory indicates that for the QD's with thicknesses beginning at 3 nm ($\approx$8.5 ML), on the other hand, the Γ-like electrons in InP are located approximately at the same energy as the X valley in the GaP matrix, implying that the electrons may localize in both materials. (We estimate that the GaP X states lie about 20 meV higher than the InP Γ valley.) For this reason, the band alignment for InP QD's embedded in a GaP matrix is expected to be either type I or a boarder case between type I and type II. Figure 2 shows the corresponding band alignment for ultrathin InP QW's and InP QD's (modeled as quantum slice). Although, a single electron is probably not strongly confined to the InP because the extended states in the GaP X valleys have similar energy to the lowest sub-band in the InP, the presence of the holes in the InP QD's results in an additional Coulomb interaction so that the exciton is relatively well spatially localized in the InP.

Williamson *et al.*, on the other hand, have calculated the electronic structure of a spherical InP QD embedded in GaP matrix.[6] According to their calculation, when the diameter of the InP QD (d_{QD}) is smaller than 6 nm, the Γ-like electrons in InP layer are localized at a higher energy than X states in the GaP layer and the band alignment of the dot is type II. Furthermore, they find that the strain in the InP/GaP system induces a new conduction-band state, which is lower in energy than both the X valley in the unstrained GaP matrix and the Γ-like electrons in the InP layer. In this way, the electrons are localized in real space at the interface between the InP QD and the GaP barrier. This new interface conduction (IC) state is indirect in reciprocal space. Therefore, an indirect transition is also predicted for larger spherical InP QD's ($d_{QD}\geqslant 6$ nm). The calculated dipole transition-matrix element between the IC state and the Γ-like holes in InP is five orders of magnitude smaller than for a typical type-I system,[6] resulting in a smaller optical transition probability and a longer carrier lifetime.

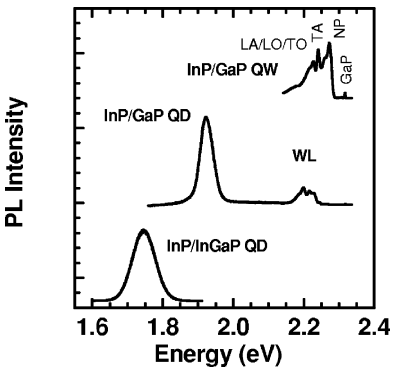

FIG. 3. Photoluminescence spectra of samples with different InP coverage measured at 5 K. For comparison, QD's in the $InP/In_{0.48}Ga_{0.52}P$ system are also shown.

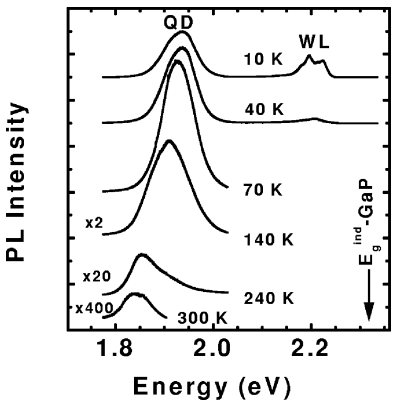

FIG. 4. Temperature dependence of the PL spectra of InP/GaP QD's resulting from 2.1-ML-InP coverage.

C. Photoluminescence

Figure 3 shows the PL spectra of two InP/GaP structures grown under high-PH_3 flux of about 1.7 sccm, together with the PL from $InP/In_{0.48}Ga_{0.52}P$ QD's (Ref. 4) shown for comparison. The top spectrum is from strained InP QW's; the InP in this structure remains 2D because the InP coverage of 0.5 ML is considerably lower than the critical thickness for dot formation (1.8 ML). The second spectrum of Fig. 3 is from a structure containing QD's formed when the InP coverage is above this critical thickness. The InP/GaP multi quantum well (MQW) sample consists of nine periods, each containing 0.5-ML-InP coverage and separated by 5 nm of GaP; the InP/GaP QD sample consists of five periods, each containing 2.1-ML InP and also separated by 5-nm GaP. The $InP/In_{0.48}Ga_{0.52}P$ sample contains a single InP deposition of 5 ML. The measurements have been carried out at 5 K with an excitation density of about 10 $W\,cm^{-2}$.

The PL emission from the two-dimensional InP-MQW samples consist of four intense and relatively narrow PL lines in the 2.15–2.20 eV range; these lines are present both in samples with only the 2D InP QW's and in samples containing QD's coexisting with the 2D InP wetting layer, but are better resolved for MQW samples. The PL from InP/GaP QD samples includes additional emission in the range of 1.9–2.0 eV and is due to the radiative recombination of heavy holes and electrons in the dots.[5] The origin of the PL line at about 2.2 eV is the wetting layer.

Also depicted in Fig. 3 is the PL spectrum from InP QD's in a $In_{0.48}Ga_{0.52}P$ matrix. This system is without question a type-I system and has also been used as the active layer in lasers.[12] The PL intensity from the InP/GaP QD's is similar in intensity to that from the $InP/In_{0.48}Ga_{0.52}P$ QD's and about 200 meV higher in energy mainly due to the band-gap difference between the different matrix materials.

We explain the photoluminescence from the 2D InP MQW's as spatially indirect recombination of electrons from the GaP *X* valleys with holes in the InP and its phonon replicas involving the phonons near the *X* points in the Brillouin zone.[8] The energy differences between the highest-energy PL line and the other three transitions are 12, 30, and 40 meV, for all samples. The energy separations between the peaks and the independence of these separations with respect to InP coverage suggest that the three emissions peaks with lower energy are phonon replicas of the highest-lying peak. The separations agree well with the transverse-acoustic, longitudinal-acoustic, and either transverse-optical or longitudinal-optical phonons near the *X* points in the GaP Brillouin zone with energies of 13.2, 30.4, and 44–45 meV, respectively.[13,14] These energies are not appreciably changed for $In_yGa_{1-y}P$ with small In mole fraction y.[13] Thus, we identify the highest-energy peak in each spectrum as the no-phonon (NP) emission and the lower energy peaks as its phonon replicas. The energies of the NP peaks agree well with calculated type-II recombination of electrons in the GaP *X* valleys with holes in the InP, as depicted in Fig. 2.

Since the wetting layer is always thinner than 3 nm (see Sec. III B), these 2D InP films in GaP could be expected to also be type II and the PL is attributed to radiative recombination of heavy holes in the InP wetting layer with electrons in the GaP *X* valleys. As noted above, however, the wetting layer could also be coupled with the QD's, leading to a more complicated situation.

We now turn our attention to the emission from the InP QD's. All PL spectra of QD samples indicate a simple Gaussian shape whose width is determined by the size distribution in a QD ensemble.[15] At low excitation density (3 $W\,cm^{-2}$), the full width at half maximum of InP/GaP QD luminescence varies between 40 and 70 meV, depending on growth conditions.

Figure 4 shows the temperature evolution of the PL from InP/GaP QD sample using an excitation density of 10 $W\,cm^{-2}$. As the temperature is increased from 5 K, the luminescence shifts from the wetting layer to the QD's due to the interplay between various capture and recombination channels. At 80 K, the PL from the wetting layer vanishes. This behavior is similar to what we observe in the InAs/GaAs system and is also reported for the GaSb/GaAs system.[16] The data of Fig. 4 also shows that the PL linewidth is rather insensitive to temperature, an observation typical for PL from QD's. In the temperature dependence of the PL, two distinct temperature regimes can be recognized. In the first regime (5–80 K), the overall PL intensity increases, whereas, in the second regime (80–300 K), it decreases (see Fig. 5). The integrated PL intensity is proportional to the number of excited electron-hole pairs that radiatively recombine. This

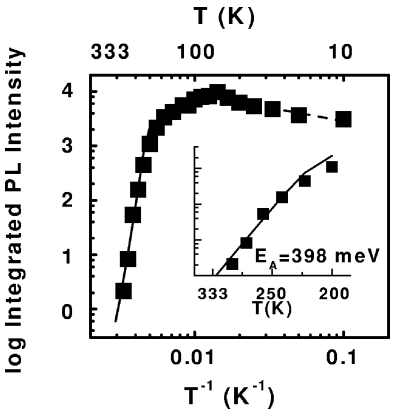

FIG. 5. Semilogarithmic plot of the integrated PL intensity versus inverse temperature. The activation energy is derived from the slope of the solid line.

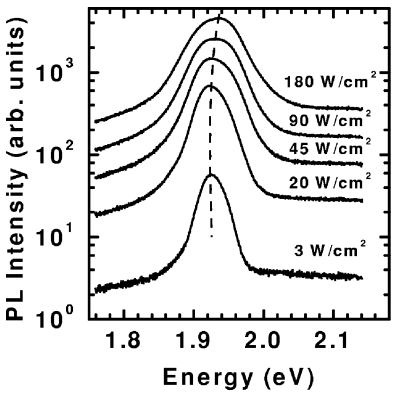

FIG. 6. PL spectra from the sample with 2.1-ML-InP coverage (under high-PH_3 flux) at different excitation densities. The dashed line shows the energy shift.

radiative recombination, and with it the total PL intensity, is determined by the following two effects.

(1) The increase of PL intensity with increasing temperature, at lower temperatures, may result from electrons that were in the GaP barrier and in the InP wetting layer thermally escaping into the QD's, where the recombination rate is much higher. On the other hand, the rise of PL intensity could also be due to the existence of QD's with type-II band alignment or existence of vacancies in the InP QD's, whose captured electrons are thermally released. In this case, the captured electrons are localized lower than Γ valley in the InP QD and recombine nonradiatively.[17] Only when the electrons can gain energy and are released into the Γ-valley state in the InP QD, for example, by thermal activation at higher temperature, the electron-hole pairs are able to recombine radiatively, resulting in the higher overall-PL intensity.

(2) The decrease in the PL intensity at higher temperatures is mainly due to thermalization of the holes out of the InP QD's into the surrounding GaP matrix, where the recombination oscillator strength is much smaller.

For temperatures below 80 K, the first effect is stronger than the second one. Therefore, we observe an increasing integrated PL intensity, whereas for temperatures above 80 K, the second effect dominates and we observe a decreasing integrated PL intensity.

Using the temperature dependence of the luminescence intensity, we determine the activation energy of heavy holes in the QD's. For temperatures higher than 220 K, the localization energy of electrons can be neglected compared to the localization energy of heavy holes. Thus, the slope of a plot for temperatures higher than 220 K gives the activation energy for heavy holes; we obtain an activation energy of 398 ± 20 meV, which is the energy difference between the heavy-hole sub-band and the valence-band discontinuity, $\Delta E_v - E_{hh1}$. This activation energy also corresponds to the energy difference between the QD luminescence and the GaP indirect band-gap, indicating that the GaP X states have approximately the same energy as the Γ-like lowest electronic sub-band in the InP (see Fig. 2) in agreement with the band alignment modeling discussed in Sec. III B.

The dependence of PL energy on excitation intensity is also useful in distinguishing type-I from type-II systems. In type-II systems, the formation of a dipole layer at the heterointerface leads to a pronounced blue shift of the PL peak.[18] This effect is also seen in type-II QD systems.[19] Figure 6 shows the PL spectra for a sample with 2.1 ML of InP coverage for excitation densities between 3 and 180 W/cm^2. Only a small energetic shift is observed, consistent with type-I QD's. This small shift is due to band filling and perhaps also due to the participation of excited states; both processes are also consistent with the increase of the emission peak width from 39 to 75 meV with increasing excitation intensity.

D. Pressure-dependent PL

To further clarify the band alignment of InP/GaP QD's, we have investigated the samples using photoluminescence measurements under hydrostatic pressure up to 10 GPa.[20] High-pressure studies of the low-temperature PL of quantum dots are a powerful method for investigating the electronic sub-band structure and have been demonstrated in InAs/GaAs (Refs. 21 and 22) and InP/$In_{0.48}Ga_{0.52}P$ (Ref. 23) systems.

At ambient pressure, the PL of the QD's is peaked at about 1.922 eV and its intensity is two orders of magnitude larger than that from the wetting layer. At a pressure between 0 and 0.30 GPa, the QD emission diminishes abruptly in intensity and the energy of the PL maximum first blue shifts by about 20 meV. As the pressure is further increased, the PL from the QD's redshifts by about 5 meV before vanishing altogether at around 1.2 GPa. Figure 7 shows the energetic position of the emission peak from the QD's as a function of hydrostatic pressure.

In our picture, as described in Sec. III B, at normal pressure, the Γ valley in the InP QD's lies at approximately the same energy as the X valleys in the adjacent GaP. The X valleys of the InP are split due to the builtin biaxial strain in the dots and the four degenerate X_{xy} valleys lie only slightly higher in energy than the Γ valley. The effect of the hydrostatic pressure is to shift the Γ point in InP to higher energy first until it lies higher than the InP X_{xy} valleys. The effect is

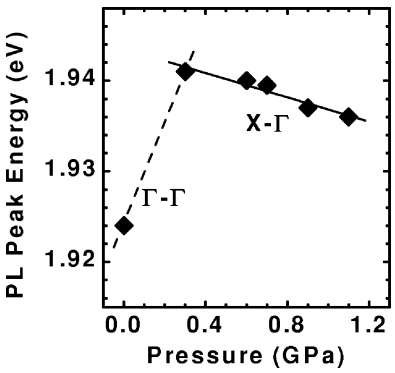

FIG. 7. Hydrostatic pressure dependence of the maximum in the PL emission from InP QD's on GaP with 2.1-ML-InP coverage (under high-PH_3 flux). The system is transformed from direct to indirect at a pressure of less than 0.3 GPa and from type I to type II for pressures greater than 1.2 GPa.

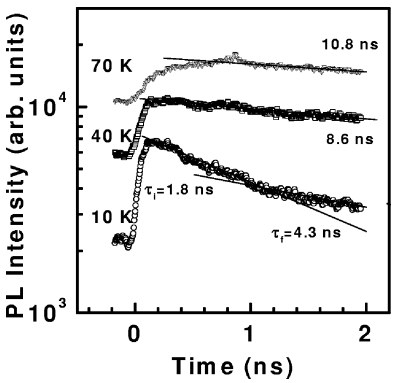

FIG. 8. The PL transients from a InP/GaP QD sample containing 2.1-ML-InP coverage at three different temperatures. The PL is excited using a photon energy of 3.1 eV and the transient is detected at peak maximum. The lines show the fits with corresponding time constants.

reflected experimentally in a blue shift and then an abrupt decrease in intensity when the material becomes indirect. The redshift of the QD-PL peak under further increase in pressure is typical for indirect transition in **k** space but spatially direct recombination processes from the conduction-band X valleys to hole states at the Brillouin-zone center.[24] As the pressure is further increased, the system undergoes a type-I to type-II transition at 1.2 GPa. The reason that the energy of the GaP X valleys is more strongly decreased by the increasing pressure than are the InP X_{xy} valleys is that the bulk moduli of GaP (88.2 GPa) and InP (71.1 GPa) are different, resulting in a decreased lattice mismatch under hydrostatic pressure. This reduced lattice mismatch reduces the energy splitting between the X_{xy} and the X_z states and thus contributes to an increase in energy of the InP X_{xy} states which partially compensates the overall decrease in energy with increasing pressure. The behavior of the PL as a function of pressure indicates that the peak at 1.922 eV (ambient pressure) corresponds to direct optical transitions between the two lowest electron and hole Γ-point states confined in the InP dots and, thus, a type-I band alignment for the InP/GaP QD's. The pressure data also allow us to determine the positions of the different conduction-band states at ambient pressure. We find that the InP X_{xy} valleys are about 20 meV above the InP Γ valley and the GaP X valleys are about 30 meV above the InP Γ valley.

E. Time-resolved PL

Further insight into the band alignment and carrier dynamics in the InP/GaP QD system can be obtained through time-resolved PL measurements. As noted above, the indirect interface state predicted in Ref. 6 leads to significantly longer carrier lifetimes than the type-I system described in Sec. III B.

The low-temperature transient (10 K) from QD's in the 2.1-ML-InP/GaP QD sample can be described as a biexponential decay with two different time constants τ_i and τ_f (Fig. 8), whereas the transient from the wetting layer can be fitted by a simple exponential decay with time constant τ_W. The initial (τ_i) and final (τ_f) decay times for the QD transient are about (2.0 ± 0.2) ns and (4.3 ± 0.2) ns, respectively. The decay times are essentially independent of detection energy between 1.9 and 1.95 eV and the observed τ_i for the other QD samples was also in the range of 2 ns. The carrier decay time in the wetting layer is about 25 ns. Additionally, we have observed for structures with two-dimensional InP MQW's, a decay time of about 20 ns.

The observed carrier lifetime of 2 ns in the InP/GaP QD's is similar to the carrier lifetimes in the range of 1–2 ns, which have been reported for type-I InAs/GaAs QD's.[25–27] On the other hand, the 2 ns is somewhat longer than our measured carrier lifetime of type-I InP/$In_{0.48}Ga_{0.52}P$ QD's, which are in the range of 100–500 ps.

Type-II systems typically show much longer carrier lifetimes as measured using time-dependent PL. As noted above, the carrier lifetime in the InP/GaP MQW samples is about 20 ns. Based on the calculation described above and on the longer lifetime, we believe that the thin QW's are type II. On the other hand, the radiative emission in these InP QW's is much more intense than one expects for a type-II transition and the pressure dependence of the wetting layer PL can also be interpreted as pointing toward a type-I, but indirect transition. In type-II GaAs/AlAs QW samples, where recombination via the higher-lying type-I Γ state also contributes, carrier lifetimes in the microsecond range were measured.[28]

The detailed time dependence of the QD PL can be understood as follows. The decay time for an isolated InP QD is about 2 ns. This time is seen in the low-temperature measurement in Fig. 8. The coupling between different QD's or different states in the QD's lead to the 4.3-ns-decay tail at longer times, similar to the InAs/GaAs case described in Ref. 27 and especially Ref. 29. At 40 and 70 K, the faster decay time of 2 ns is masked by the long rise time of the carrier concentration in the QD's. The capture of carriers into the dots is due to the thermally activated transfer of carriers from the GaP matrix and the wetting layer and is assisted by acoustic phonons to conserve crystal momentum. The thermally activated increase in carrier concentration in the QD's is also reflected in the three fold increase in luminescence intensity at 80 K compared to 10 K.

As noted above, although the decay time of 2 ns is significantly shorter than one can expect for a type-II system, it is also longer than the 500 ps time measured in the $InP/In_{0.48}Ga_{0.52}P$ QD system. This difference is not difficult to understand when one considers that the *X* states of the GaP lie only 30 meV higher in energy than the Γ states of the InP, and the Bloch part of the excitonic wave function contains an admixture of Bloch states including components from the GaP *X* states. In this way, the matrix element coupling the electron and hole wave functions is reduced as compared to that in the $InP/In_{0.48}Ga_{0.52}P$ QD system, where the electronic part of the wave function is derived to a greater extent from the InP Γ states and the admixed barrier states are also located at Γ.

Thus, the time-dependent PL measurements are also consistent with the InP/GaP QD system being a direct and type-I system, but with conduction-band states in the GaP lying not much higher in energy. This result is entirely consistent with the other measurements of this system: The intensity of the stationary PL, its temperature dependence, its dependence on excitation intensity, and its pressure dependence.

IV. CONCLUSION

Photoluminescence from self-assembled InP quantum dots in GaP is demonstrated and investigated, together with their growth and structural properties. The QD's are prepared using gas-source MBE and appear to form via the Stranski-Krastanow mechanism after a critical InP coverage of 1.8 ML is reached. A two-dimensional InP wetting layer coexists with the InP QD's as is usual in Stranski-Krastanow processes.

InP deposition below the critical thickness for QD formation results in strained InP QW's which also luminesce strongly between 2.17 and 2.28 eV. This emission results from the spatially indirect recombination of electrons from the GaP *X* valleys with holes in InP and several phonon replicas. The energy of the no-phonon line of each PL spectrum can be calculated using a realistic multi-valley effective-mass approximation calculation based on a type-II band alignment and coupled wells. That the band alignment is type II is further confirmed by the carrier lifetime of about 20 ns, which is much longer than in direct band-gap type-I systems.

The InP deposition greater than the critical thickness for dot formation results in InP islands whose size is dependent on the growth conditions. Supercritical InP deposition under a sufficiently high-PH_3 flux results in relatively small and dense dots with optical emission peaks between 1.9 and 2.0 eV, depending on InP coverage. This energy is 0.5 eV higher than the InP bulk band gap due to strain, quantum confinement, and, to some extent, perhaps Ga interdiffusion. This luminescence persists to above room temperature, but decreases in intensity due to the holes being thermally excited out of the QD's. A theoretical model of the band alignment between the strained InP and the GaP matrix predicts that the *X* valley of the GaP is approximately in alignment with the Γ valley of the InP. Results from pressure-dependent PL experiments, furthermore, indicate that the optical emission results from recombination which is direct in both real and **k** space of electrons in the InP Γ valley with holes also in the InP Γ valley. The pressure dependence of the PL further indicates that at ambient pressure, the lowest *X* states in the InP lie about 20 meV higher than the Γ valley and the GaP *X* valleys are some 30 meV higher. The direct band gap and type-I character of the recombination is also supported by the observed carrier lifetime in the QD's of about 2 ns, a value consistent with type-I systems. Exploiting the visible direct-band-gap transition in the GaP system could lead to an increased efficiency of light emission in GaP-based light emitters.

ACKNOWLEDGMENTS

The authors thank K. Braune for AFM measurements, H. Kirmse for TEM measurements, H.-Y. Hao, H.T. Grahn for time-resolved measurements of quantum well structures, and G.G. Tarasov for useful discussions.

*Electronic address: hatami@physik.hu-berlin.de

[1] Y. Nabetani, K. Sawada, Y. Furukawa, A. Wakahara, S. Noda, and A. Sasaki, J. Cryst. Growth **193**, 470 (1998).

[2] B. Junno, T. Junno, M.S. Miller, and L. Samuelson, Appl. Phys. Lett. **72**, 954 (1998).

[3] R. Leon, C. Lobo, T.P. Chin, J.M. Woodall, S. Fafard, S. Ruvimov, Z. Liliental-Weber, and M.A. Stevens Kalceff, Appl. Phys. Lett. **72**, 1356 (1998).

[4] F. Hatami, U. Müller, H. Kissel, K. Braune, R-P. Blum, S. Rogaschewski, H. Niehus, H. Kirmse, W. Neumann, M. Schmidbauer, R. Köhler, and W.T. Masselink, J. Cryst. Growth **216**, 26 (2000).

[5] F. Hatami, L. Schrottke, and W.T. Masselink, Appl. Phys. Lett. **78**, 2163 (2001).

[6] A.J. Williamson, A. Zunger, and A. Canning, Phys. Rev. B **57**, R4253 (1998).

[7] C.G. Van de Walle, Phys. Rev. B **39**, 1871 (1989).

[8] F. Hatami, G. Mussler, M. Schmidbauer, L. Schrottke, H.-Y. Hao, H.T. Grahn, and W.T. Masselink, Appl. Phys. Lett. **79**, 2886 (2001).

[9] A.S. Saada, *Elasticity: Theory and application* (Krieger Publishing, Malabar, FL, 1989).

[10] S. Adachi, J. Appl. Phys. **53**, 8775 (1982).

[11] N.N. Ledentsov, M. Grundmann, N. Kirstaedter, O. Schmidt, R. Heitz, J. Böhrer, D. Bimberg, V.M. Ustinov, V.A. Shchukin, A.Yu. Egorov, A.E. Zhukov, S. Zaitsev, P.S. Kopev, Zh.I. Alferov, S. Ruvimov, P. Werner, U. Gösele, and J. Heydenreich, Solid-State Electron. **40**, 785 (1996).

[12] M.K. Zundel, N.Y. Jin-Phillipp, K. Eberl, T. Riedl, E. Fehrenbacher, and A. Hangleiter, Appl. Phys. Lett. **73**, 1784 (1998).

[13] P. Merle, D. Auvergne, H. Mathieu, and J. Chevallier, Phys. Rev. B **15**, 2032 (1977).

[14] H. Mathieu, P. Merle, and E.L. Ameziane, Phys. Rev. B **15**, 2048 (1977).

[15] W-Y. Wu, J.N. Schulman, T.Y. Hsu, and U. Efron, Appl. Phys. Lett. **51**, 710 (1987).

[16] F. Hatami, N.N. Ledentsov, M. Grundmann, J. Böhrer, F. Heinrichsdorff, M. Beer, D. Bimberg, S. Ruvimov, P. Werner, U. Gösele, J. Heydenreich, U. Richter, V. Ivanov, B.Ya. Meltser, P.S. Kopev, and Zh.I. Alferov, Appl. Phys. Lett. **67**, 656 (1995).
[17] M. Jaros and S. Brand, Phys. Rev. B **14**, 4494 (1976).
[18] H. Kroemer and G. Griffiths, IEEE Electron Device Lett. **4**, 20 (1983).
[19] F. Hatami, M. Grundman, N.N. Ledentsov, F. Heinrichsdorff, R. Heitz, J. Böhrer, D. Bimberg, S. Ruvimov, P. Werner, S.V. Ivanov, B.Ya. Meltser, V. Ustinov, P.S. Kop'ev, and Zh.I. Alferov, Phys. Rev. B **57**, 4635 (1998).
[20] A.R. Goñi, C. Kristukat, F. Hatami, S. Dressler, W.T. Masselink, and C. Thomsen, Phys. Rev. B (to be published).
[21] G.H. Li, A.R. Goñi, C. Abraham, K. Syassen, P.V. Santos, A. Cantarero, O. Brandt, and K. Ploog, Phys. Rev. B **50**, 1575 (1994).
[22] G.H. Li, A.R. Goñi, K. Syassen, O. Brandt, and K. Ploog, Phys. Rev. B **50**, 18 420 (1994).
[23] C. Ulrich, S. Ves, A.R. Gõni, A. Kurtenbach, K. Syassen, and K. Eberl, Phys. Rev. B **52**, 12 212 (1995).
[24] A.R. Goñi, K. Syassen, K. Strössner, and M. Cardona, Phys. Rev. B **39**, 3178 (1989).
[25] R. Heitz, M. Veit, N.N. Ledentsov, A. Hoffmann, D. Bimberg, V.M. Ustinov, P.S. Kop'ev, and Zh.I. Alferov, Phys. Rev. B **56**, 10 435 (1997).
[26] R. Heitz, A. Kalburge, Q. Xie, M. Grundmann, P. Chen, A. Hoffmann, A. Madhukar, and D. Bimberg, Phys. Rev. B **57**, 9050 (1998).
[27] G.G. Tarasov, Yu.I. Mazur, Z.Ya. Zhuchenko, A. Maassdorf, D. Nickel, J.W. Tomm, H. Kissel, C. Walther, and W.T. Masselink, J. Appl. Phys. **88**, 7162 (2000).
[28] P. Dawson, K.J. Moore, C.T. Foxon, G.W. 't Hooft, and R.P.M. van Hal, J. Appl. Phys. **65**, 3606 (1989).
[29] J. W. Tomm, T. Elsaesser, Yu. I. Mazur, H. Kissel, G. G. Tarasov, Z. Ya. Zhuchenko, and W. T. Masselink, Phys. Rev. B (to be published).